IJR International Journal of Railway
Vol. 3, No. 2 / June 2010, pp. 60-67

The Korean Society for Railway

A Basic Study on Wheel Flange Climbing using Model Wheelset

Yosuke Nagumo*, Katsuya Tanifuji† and Junichi Imai*

Abstract

This paper deals with an experimental study on the wheel flange climbing of railway vehicles, which is a major factor leading to derailment. An experiment is carried out on a 1/5-scale model wheelset of a truck used on a standard-gauge track, which is placed on a roller rig. The lateral external force acting on the wheelset is ramped up until derailment occurs under the condition of a fixed attack angle and wheel-load unbalance ratio. Three parameters, the height of wheel lift, the lateral force, and the wheel load acting on the outer rail, are measured until derailment occurs. From these measurements, it is possible to observe the behavior of the wheelset and to elucidate how the attack angle, the wheel-load unbalance ratio and the lateral external force affect flange-climb derailment. Then, a numerical simulation is carried out using an analytical model based on a single wheelset. As a result, the flange-climb behavior observed in the experiment can be explained theoretically on the bases of the analytical results, although further improvement of the model is desired.

Keywords **:** *Analytical model, Numerical simulation, Railway, Derailment, Flange climbing, Scaled model, Wheelset*

1. Introduction

The derailment of rail vehicles is a critical issue to their running safety. One of the factors leading to accidents involving the derailment of rail vehicles in recent years is wheel flange climbing [1]. When a rail vehicle runs on a curve at a low speed, the outer wheel load of the leading axle can be reduced by excessive cant or twisting of the track surface along the exit transition curve. Under such conditions, the wheel can climb the rail and derailment may occur owing to the existence of a lateral force and a high frictional coefficient. This phenomenon is known as "wheel-climb derailment". The process leading to derailment is roughly divided into two stages. In the first stage, during which the wheel is in contact with the rail at two points, the tread and flange, the vertical load on the wheel tread decreases to zero and the wheel becomes in contact with the rail only at the flange. In the second stage, the flange climbs the rail and derailment occurs. The behavior of the wheelset in the second stage has not yet been adequately clarified, and further investigation is required [2].

In this paper, flange-climb derailment is investigated experimentally using a scale-model wheelset. Utilizing the model apparatus, the derailment phenomenon, which is difficult to measure or replicate, can be investigated relatively easily. An experimental study using the model apparatus has recently been reported by Nagase et al. [3], in which the actual running of a reduced-scale two-axle truck was executed on a reduced-scale experimental rail track. Braghin et al. reported an experimental study on the derailment using a full-size single-axle truck on a roller rig [4]. Using a single-wheelset model, Ishida et al. analytically investigated the derailment of a high-speed rail vehicle under high-frequency wheel load variation [5]. However, there are few reports in which the values of each wheelset parameter, which are regarded as having a strong effect on the flange-climb behavior, are varied independently, or in which the difference in the behavior resulting from the variation of these parameters is investigated. Thus, we carried out an experimental study on the flange-climb phenomena, using a reduced-scale model. In this study, we investigate the flange-climb behavior leading to the derailment of a single-axle truck on an experimental roller rig while varying the various parameter values. Then, an ana-

† Corresponding author: Department of Mechanical and Production Engineering, Niigata University, Japan
E-mail: tanifuji@eng. nigata-u.ac.jp
* Department of Mechanical and Production Engineering, Niigata University, Japan

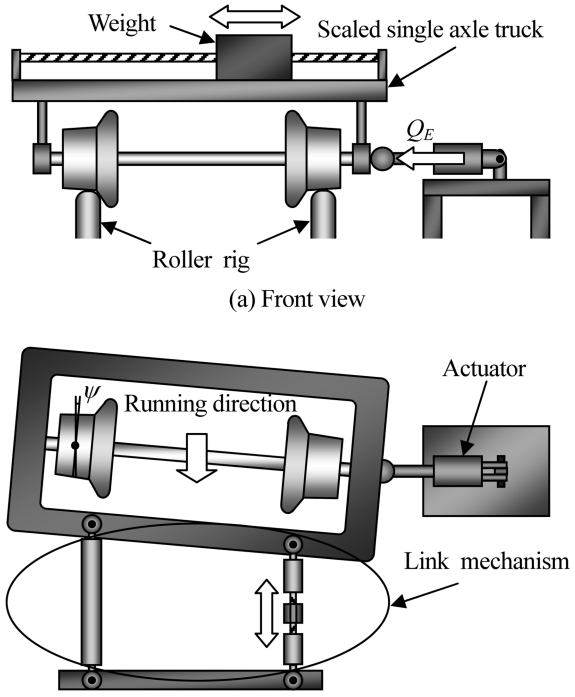

Fig. 1 Outline of experimental apparatus

lytical model of the single-axle truck is developed and a numerical analysis is carried out to compare the results obtained experimentally and by analysis.

2. Experiment

2.1 Apparatus

Fig. 1 shows an outline of the test apparatus. The wheels of a 1/5-scale single-axle truck used on a standard-gauge track are placed on a roller rig rotating at a constant speed. The running direction is indicated with an arrow in the plan view. The wheel load can be varied by moving a weight on the truck frame in the lateral direction; thus, the wheel-load unbalance ratio between the left and right wheels can be set arbitrarily.

The wheel-load unbalance ratio used in this paper is defined by the loads on the left and right wheels divided by half the weight of the single-axle truck in the stationary condition. Thus, this ratio is different from that under running conditions with the application of an external force. Hereafter, the wheel-load unbalance ratio, written as r_p, represents that of the wheel on the outer rail.

The attack angle of the wheelset, ψ, is fixed arbitrarily using a link mechanism as shown in Fig. 1(b). The lateral external force Q_E acting on the wheelset is applied to the

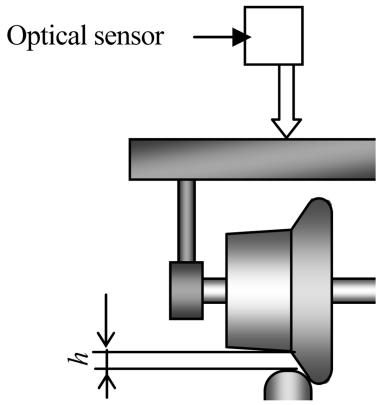

Fig. 2 Measurement of wheel lift

axle box by a hydraulic actuator, thus the effect of its pressurization on the wheel load is small. These mechanisms make it possible to simulate the flange contact condition of the outer wheel along a curved track.

The measurable parameters in the experiment are the wheel lift height, the left and right wheel loads, and the wheel lateral force. Here, the wheel lift height h is the height of flange climbing and can be obtained indirectly by measuring the vertical displacement of the truck frame above the wheel using an optical displacement sensor as shown in Fig. 2. Wheel loads and lateral forces are obtained from the output of strain gauges attached on the eight spokes of each rail wheel by the continuous measuring method [6].

2.2 Methodology

In the experiment, flange-climb derailment is caused by slowly increasing the lateral external force under the condition that the attack angle and wheel-load unbalance ratio are fixed. The running speed is set to a low speed corresponding to 10 km/h for actual-size vehicles based on the similarity law. The attack angle ψ is set to one of four values: 5, 10, 15 or 20 mrad. It has been reported that the stationary attack angle is less than 1 deg (= 17.5 mrad) when an ordinary two-axle bogie vehicle negotiates a curve with a radius of more than 200 m [7].

The wheel-load unbalance ratio r_p is varied from 1.0, which corresponds to an equal load on the left and right wheels, to 0.3, which is the minimum value of r_p that can be set using the experimental apparatus, in increments of 0.1. To observe the characteristic behavior of flange climbing, the experiment is carried out under the extreme condition of r_p = 0.3. The applied lateral external force Q_E is ramped up from an initial value of 0 N/s at a rate of 50 N/s. In practice, the external force begins to act after a few seconds as shown in Fig. 3, because there is a gap between

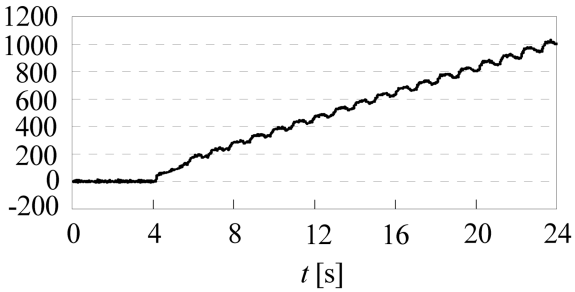

Fig. 3 Lateral external force applied during experiment

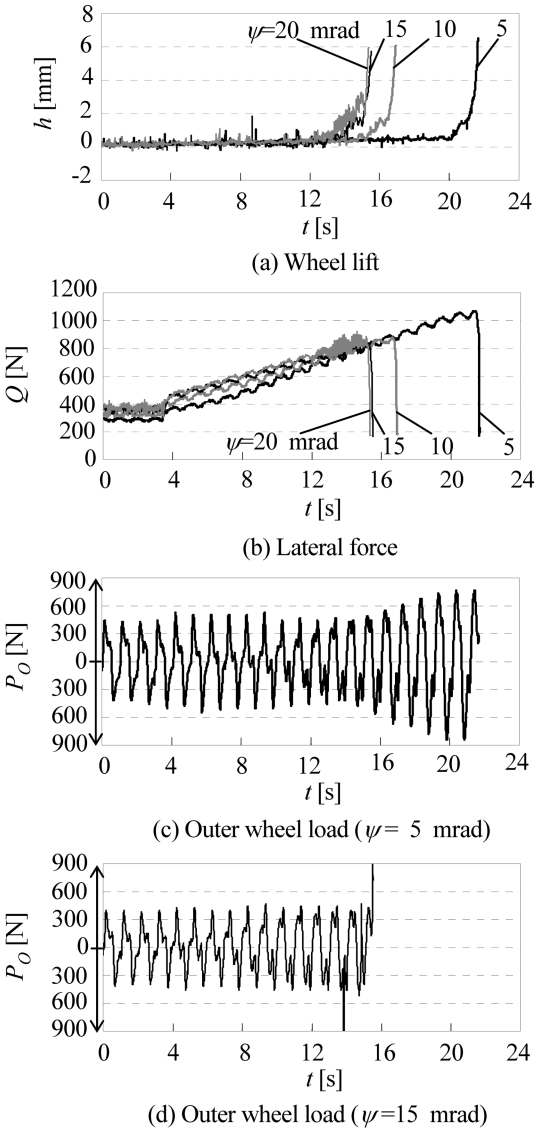

Fig. 4 Experimental results for wheel-rail interaction (r_p= 0.7)

the axle box and the actuator.

The measurement of wheelset behavior starts from the moment when the actuator is applied until derailment occurs. To minimize the variation in the experiment results, the measurement is performed five times under each condition.

2.3 Results

Fig. 4 shows the experimental results obtained for r_p = 0.7. The waveforms correspond to each attack angle ψ. Graph (a) represents the waveform of wheel lift h, graph (b) shows the lateral force Q acting on the outer wheel and graphs (c) and (d) show the load acting on the outer wheel P_O for two attack angles separately for clarity. Here, the measurement parameters for the inner wheel are omitted so that attention can be focused on the behavior of the outer wheel.

The wheel flange climbs until derailment occurs with increasing time, as shown in Fig. 4(a). Derailment occurs when the wheel lift reaches 6 mm, which corresponds to the flange height of the model wheel. With increasing ψ, the time required for derailment decreases, and there is negligible difference between the results for ψ = 15 and 20 mrad.

The value of the wheel lateral force Q can be obtained from the peak height of the waveform shown in Fig. 4(b). Q increases monotonically with time, and the sudden decrease in Q implies that the wheel was derailed. Here, with increasing ψ, the value of Q decreases at the moment when derailment occurs. Moreover, each lateral force remains constant for the first 4 s because the external force Q_E does not act in this time period.

Fig. 4(c) and 4(d) show the outer wheel load P_O when ψ = 5 and 15 mrad, respectively. The vertical axes indicate positive values in both the positive and negative directions, because the wheel repeatedly takes positive and negative values with each rotation of the rail-wheel. Here, the continuous measuring method has a drawback that the wheel load is sensitive to noise. Then, we read off the peaks of the waveform smoothly. When ψ=5 mrad, P_O initially increases slightly and decreases temporarily at about t=12 s, then increases rapidly after t=14 s, leading to derailment. On the other hand, when ψ=15 mrad, P_O remains constant up to derailment.

Fig. 5 shows the waveforms when r_p=0.9, 0.7, 0.5 and 0.3, with ψ fixed at 15 mrad. It is shown from Figs. 5(a) and 5(b) that the time required for derailment decreases when r_p decreases. Figs. 5(c) and 5(d) show the outer wheel load P_O when r_p=0.5 and 0.9, respectively. When r_p =0.9, P_O exhibits similar behaviour to that in Fig. 4(c), and when r_p=0.5, P_O increases monotonically from the time when the external force begins to act.

Fig. 6(a) shows the external force Q_E required for derailment and Fig. 6(b) shows the derailment coefficient Q/P at the moment when wheel lift first occurs, for each wheel-

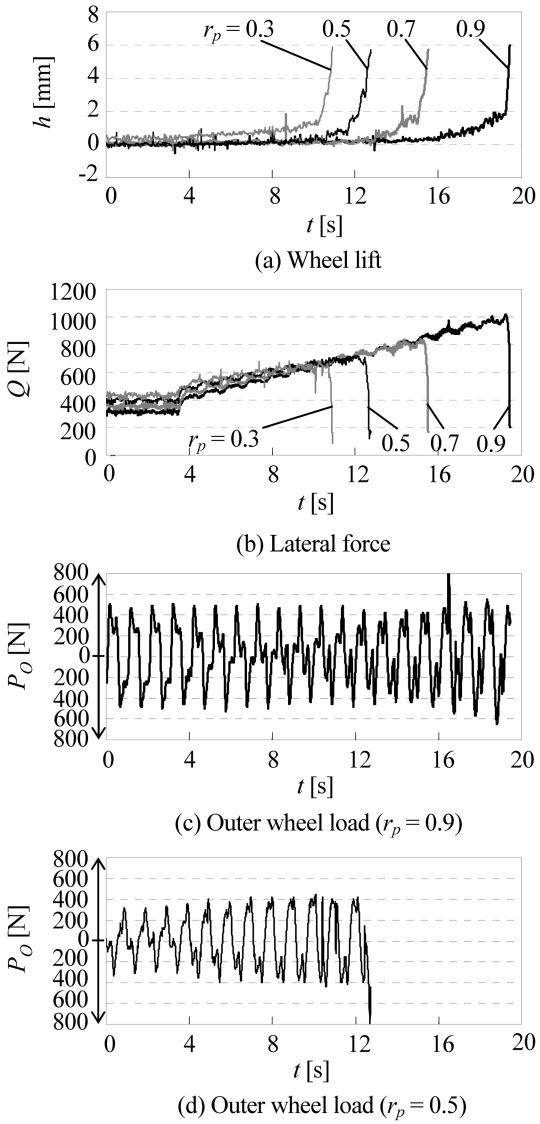

Fig. 5 Experimental results for wheel-rail interaction (ψ= 15 mrad)

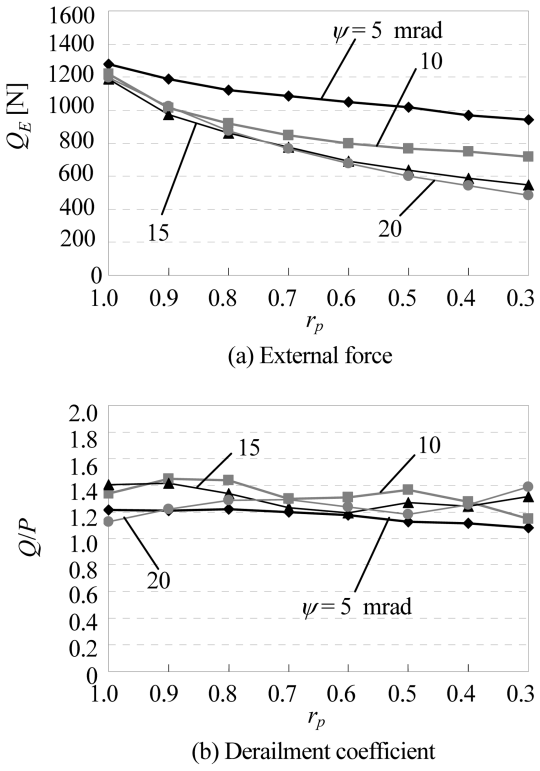

Fig. 6 (a) External force required for derailment in experiment and (b) derailment coefficient at the time of wheel lift, for each wheel-load unbalance ratio r_p

load unbalance ratio r_p and attack angle ψ. As shown in Fig. 6(a), the external force required for derailment tends to decrease with increasing attack angle ψ and decreasing r_p.

When r_p = 1.0, there is little difference in Q_E with changing attack angle, however, as r_p decreases, the difference becomes larger. Regarding the derailment coefficient Q/P in Fig. 6(b), no definite tendency can be observed upon changing ψ and r_p. In particular, the fluctuation of Q/P by the change in ψ was small in the case of r_p = 0.7, the case illustrated in Fig. 4. Here, when ψ decreases, the wheel load P increases owing to the increase in the external force Q_E, which is required for wheel flange climbing (refer to Eq. (1)).

To summarize this section, the behavior of a wheelset leading to derailment as it negotiates a curve has been observed experimentally using a single-axle truck on a roller rig. From the experiment, the effect of the attack angle ψ, the wheel-load unbalance ratio r_p and the external force Q_E on the phenomenon of wheel flange climbing were clarified.

3. Numerical Analysis

3.1 Forces Acting on Wheelset

For comparison with the experimental results, a numerical simulation is carried out by developing an analytical model. The weight of the single wheelset in the model includes the weight of the truck frame used in the experiment. Similar to the experiment in which the attack angle ψ is fixed, lateral motion y is the only degree of freedom allowed. When an external force Q_E is applied in the leftward direction, the wheelset is laterally displaced, resulting in two-point contact of the left wheel with the rail. Setting the lateral displacement at the neutral position as y=0, the forces acting on the wheelset are shown in Fig. 7. In this situation, the load P_l acting on the left tread is given by Eq. (1), which is obtained from the equilibrium of

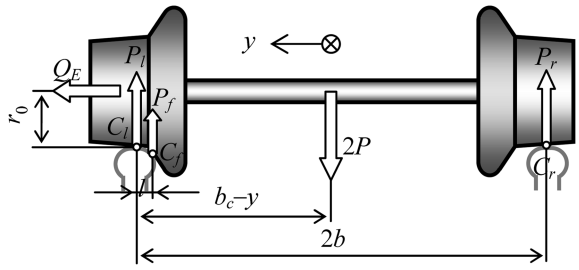

Fig. 7 Forces acting on wheelset

moments about the contact point C_r.

$$P = \frac{2b-(b_c-y)}{b}P - \frac{2b-l}{2b}P_f + \frac{r_0}{2b}Q_E \tag{1}$$

Here, b represents half the distance between the contact points on the right and left treads, b_c is the lateral distance between contact point on the left tread and the center of gravity of the wheelset, l is the distance between the contact points on the tread and flange of the left wheel, r_0 is the wheel radius, P is half the weight of the wheelset, and P_f is the vertical load at the contact point on the flange.

Fig. 8 shows the forces acting on the contact point on the flange: (a) shows the condition before flange climbing occurs and (b) shows that during flange climbing. Under the condition of two-point contact shown in Fig. 8(a), the flange reaction force Q_f, which is equal to the sum of the external force Q_E and the sum of lateral creep forces F_2 ($=F_{2tl}+F_{2tr}$) acting on the right and left wheel treads, acts at the contact point on the flange, and the corresponding vertical component P_f is obtained from Eq. (2).

$$P_f = \frac{Q_f}{\tan\alpha} = \frac{Q_E+F_{2tr}}{\tan\alpha} \tag{2}$$

For an attack angle ψ, the lateral creep force F_{2tl} also acts on the tread of the flanging wheel. Thus, the wheel lateral force Q is calculated by the subtraction of F_{2tl} from the flange reaction force Q_f, as shown in Eq. (3).

$$Q = Q_f - F_{2tl} = Q_E + F_{2tr} \tag{3}$$

The outer wheel load P_O is equal to the sum of P_l and P_f.

$$P_O = P_l + P_f \tag{4}$$

Here, the lateral creep force is calculated using Hertzian theory [8] and Kalker's nondimentional coefficient [9]. The asymptotic approach of the creep force toward the frictional force is modeled using the Lévi and Chartet formulation [10].

The condition that the tread load P_l becomes zero corresponds to the situation of wheel lift, as shown in Fig. 8(b). Here, the wheel is only in contact with the rail at the flange and the vertical component P_f of the force acting on

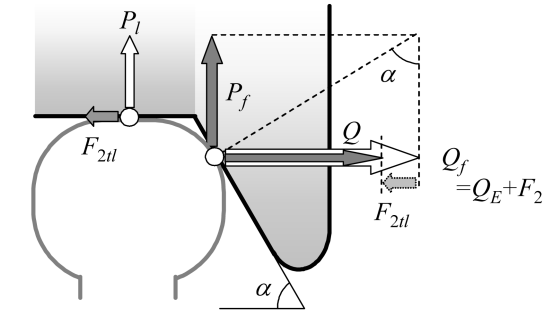

(a) Under condition of two-point contact

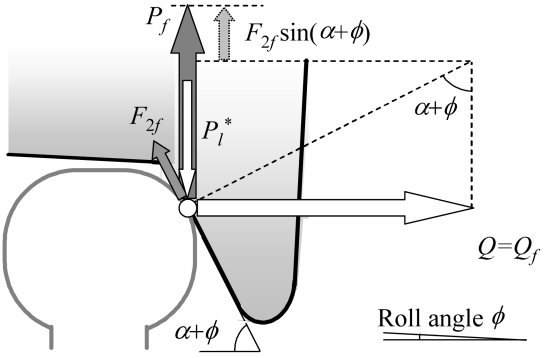

(b) During flange climbing

Fig. 8 Forces acting between wheel and rail

the contact point is equal to the sum of the vertical components of the flange reaction force Q_f and the lateral creep force F_{2f} acting on the flange.

$$P_f = \frac{Q_f}{\tan(\alpha+\phi)} + F_{2f}\sin\alpha \tag{5}$$

The difference between the vertical force P_f in Eq. (5) and the wheel load P_l* on the flange gives an upward force ΔF, which is given by Eq. (6). ΔF acts parallel to the flange taking the upward direction as positive.

$$\Delta F = Q_f\cos(\alpha+\phi) + F_{2f} - P_l^*\sin(\alpha+\phi) \tag{6}$$

Here, it can be considered that flange climbing occurs when ΔF becomes positive.

3.2 Modeling of Flange Climbing

An equation of motion for the wheelset model is derived using the forces obtained in the preceding section. Generally speaking, the lateral motion y is considered as a degree of freedom of the wheelset. In this study, however, the degree of freedom is altered to the roll motion ϕ about the contact point C_r on the tread of the right wheel, as shown in Fig. 9, since the behavior during flange contact is focused on in this

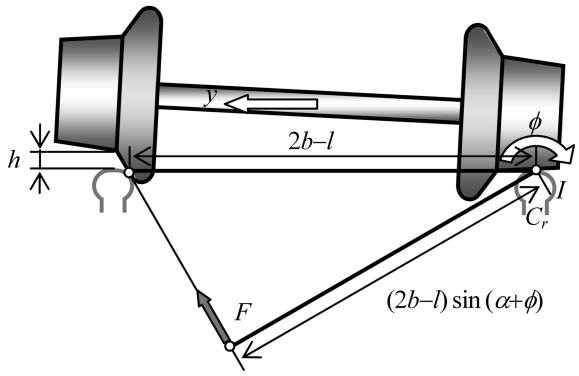

Fig. 9 Analytical model of wheelset used to investigate flange climbing

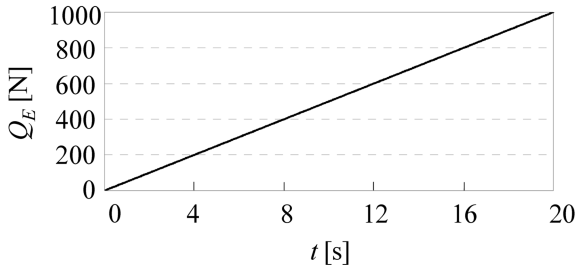

Fig. 10 Lateral external force applied in numerical simulation

study. The equation of motion is given in Eq. (7).

$$I\ddot{\phi} = (2b-l)\sin(\alpha+\phi)\times F \tag{7}$$

Here, I denotes the moment of inertia of the wheelset about the point C_r and F is the resultant force acting parallel to the flange. F is classified into the following five cases depending on the height of wheel lift h and the value of ΔF given by Eq. (6).

Case 1. $\Delta F \geq 0 : F = \Delta F$

Case 2. $h = 0, \Delta F < 0 : F = 0$

Case 3. $h > 0, \Delta F < 0, |\Delta F| \geq \mu N :$

$$F = \Delta F + \mu N$$

Case 4. $h > 0, \Delta F < 0, |\Delta F| < \mu N, \dot{h} > 0 :$

$$F = \Delta F - \mu N$$

Case 5. $h > 0, \Delta F < 0, |\Delta F| < \mu N, \dot{h} \leq 0 :$

$$F = 0$$

When ΔF is positive, F becomes equal to ΔF like Case 1, and wheel climbs with the flange adhering to the rail. Case 2 corresponds to the condition before wheel lift occurs, where h remains equal to zero and F is set to zero even if ΔF is negative. Case 3 to Case 5 correspond to conditions after the initial occurrence of wheel lift. In Case 3, F becomes negative and the wheel slips down. In Case 4, F is negative, causing the upward speed of the wheel to decrease. In Case 5, F becomes zero and the wheel stops climbing.

3.3 Analytical Method

The parameter values of the model are adjusted to those of the experimental apparatus, and the conditions used in the analysis are set to those of the experiment. The frictional coefficient between the wheel tread and the rail is taken as $\mu = 0.25$, considering the rust and contaminants attached on the experimental apparatus. In addition, $\mu = 0.15$ is used for the contact point on the flange, since the flange surface is assumed to include more contaminants. In the analysis, an external force is applied, which is ramped up in accordance with the ideal curve in Fig. 10, starting from $t = 0$. When the wheel lift h reaches 6 mm, which corresponds to the flange height and the occurrence of derailment, the calculation is stopped.

3.4 Comparison with Experimental Results

Fig. 11 shows the simulated waveforms illustrating the effect of attack angle ψ. Graphs (a), (b) and (c) correspond to the experimental results in (a), (c) and (d) of Fig. 4, respectively. In graph (a), the wheel lift shows a similar trend to that observed experimentally. Here, the difference between the times until derailment for $\psi = 15$ and 20 mrad is small. This is because the lateral creep force approaches the value of the saturated frictional force. It is presumed that this characteristic tendency appeared in the experiment. It is also observed that gradual wheel lift occurs until $h = 0.5$ mm which is followed by rapid wheel lift. When $h < 0.5$ mm, the contact point between the wheel and the rail is at the flange root, where the contact angle is small. Thus, the wheel lift up to $h = 0.5$ mm can occur easily. When h reaches 0.5 mm, the wheel temporarily stops rising because the contact point moves to the main part of the flange where the contact angle is large. After that, with increasing lateral external force, the wheel flange gradually climbs the rail. When the contact point moves close to the flange top, the contact angle becomes small and derailment occurs rapidly.

In Figs. 11(b) and 11(c), the wheel load P_O temporarily decreases at approximately $t = 6$ s. This is because the contact point moved to the region on the flange where the frictional coefficient is low and the lateral creep force F_{2f} is decreased. Then, P_O tends to increase with increasing lateral external force Q_E, under which F_{2f} causes the outer

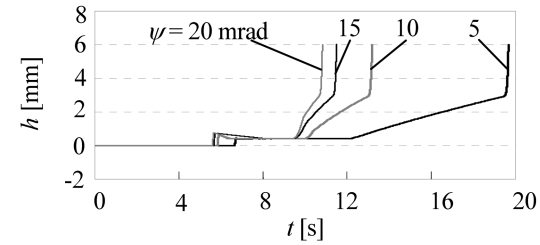

(a) Wheel lift

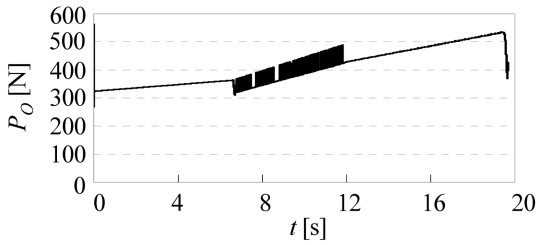

(b) Outer wheel load (ψ = 5 mrad)

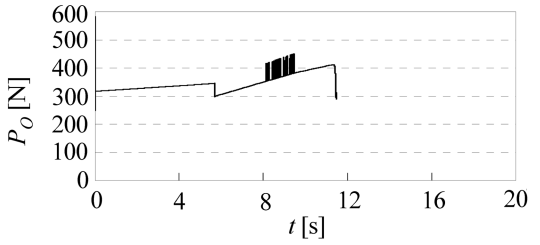

(c) Outer wheel load (ψ = 15 mrad)

Fig. 11 Analytical results on wheel-rail interaction (r_p = 0.7)

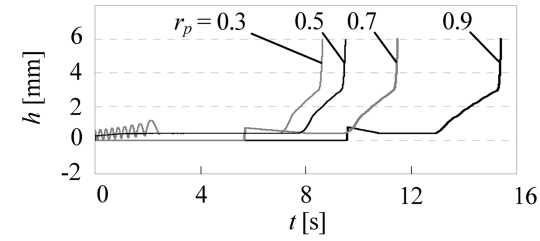

(a) Wheel lift

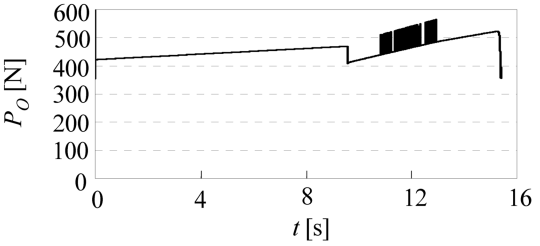

(b) Outer wheel load (r_p = 0.9)

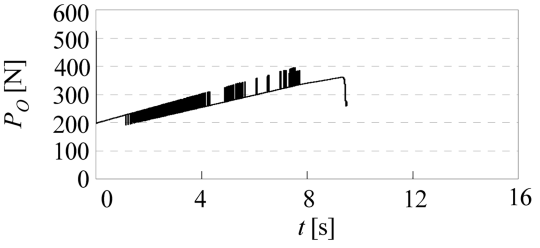

(c) Outer wheel load (r_p = 0.5)

Fig. 12 Analytical results on wheel-rail interaction (ψ = 15 mrad)

wheel load to increase. Similar behavior for P_O was also observed in the experiment and is considered to have the same cause. However, no significant increase in P_O can be observed in Fig. 4(d). This is because the time from the start of flange climbing until derailment is very short.

Fig. 12 shows the simulated waveforms illustrating the effect of wheel-load unbalance ratio r_p. The waveforms in Fig. 12 exhibit similar behavior to those in Fig. 5, where the observed behavior caused by the increase in lateral external force Q_E can be explained similarly to that given for the results shown in (a) and (b) in Fig. 11. For a large wheel-load unbalance ratio such as r_p=0.5 in Fig. 12(c), P_O rises relatively rapidly from the time the external force begins to act. Here, wheel lift occurs without the effect of the external force, as indicated in Fig. 12(a), and also the lateral creep force acting on the inner wheel tread increases with time. This behavior is consistent with the experimental result shown in Fig. 5(d) after the external force begins to act.

Fig. 13(a) shows the theoretically obtained external force required for derailment and Fig. 13(b) shows the derailment coefficient required for wheel lift for various values of r_p and ψ. These graphs correspond to the experimental results shown in Fig. 6. It can be seen in Fig. 13(a) that the external force required for derailment tends to decrease with increasing ψ and with decreasing r_p, consistent with the experimental results in Fig. 6(a). Therefore, it is demonstrated that the analytical model is suitable for performing qualitative simulations. However, in the experiment, the effect of ψ is small when r_p is large and becomes large as r_p decreases, which differs from the trends observed in the numerical analysis. Thus, the results of analysis are not in satisfactory quantitative agreement with the experimental results, and it is considered that the model requires further improvement. Fig. 13(b) shows that r_p has little effect on the derailment coefficient Q/P, which remains in the range from 1.3 to 1.6 with changing r_p, which is reasonably consistent with the experimental result shown in Fig. 6(b). However, the tendency that Q/P decreases with increasing ψ is different from that observed in the experiment. In addition, the values of Q/P obtained in the experiment are generally smaller than those obtained in the

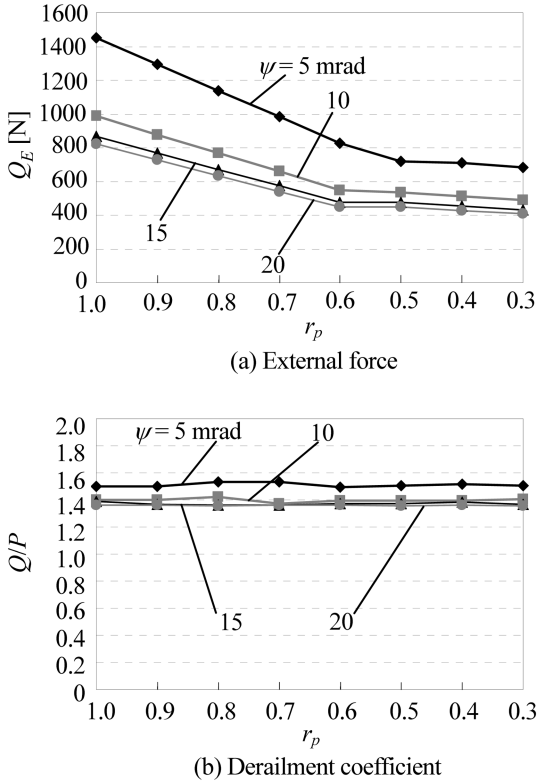

Fig. 13 (a) External force required for derailment in numerical simulation and (b) derailment coefficient at the time of wheel lift, in each wheel-load unbalance ratio r_p

numerical simulation, which is considered to be caused by the difference between the frictional coefficient μ in the experiment and the numerical analysis. From the estimation of μ using Nadal's formula (Eq. (8))[11], it can be inferred that the frictional coefficient μ of the model wheel, the flange angle of which is α=70 deg, fluctuates in the range between 0.3 and 0.4.

$$\frac{Q}{P} = \frac{\tan\alpha - \mu}{1 + \mu\tan\alpha} \tag{8}$$

As mentioned above, the analytical model developed in this study enabled the experimental results to be considered theoretically.

4. Conclusion

In this paper, to elucidate the flange-climb behavior of a wheelset, derailment experiments using a model wheelset and numerical simulations were carried out. The obtained results are as follows:

(1) In the experiment, the flange-climb behavior until derailment was observed by measuring the height of wheel lift, the wheel load and the wheel lateral force.

(2) From the experimental results, the effects of the attack angle, the wheel-load unbalance ratio and the lateral external force on flange climbing were clarified.

(3) The flange-climb behavior obtained in the experiment was considered by comparing the results of the numerical simulation and the experiment.

New insight into the mechanism of wheel flange climbing was obtained. However, although the analytical model developed for analyzing the wheel flange climbing can simulate the behavior of the wheelset qualitatively, further improvements to the model are required to reduce the quantitative discrepancy between the theoretical and experimental results by considering such as the forward shift of the contact point on the flange caused by the attack angle.

Reference

1. Maruyama, H. and Kageyama, N. (1981). "Railway engineering for mechanical engineers (in Japanese)," Maruzen, pp. 117-120.
2. Railway Accident Investigation Committee (2000). Research Report on Derailment and Collision Accident at Nakameguro Station of Eidan Subway Hibiya Line (in Japanese), pp. 1-107, Railway Accident Investigation Committee.
3. Nagase, K., Sakahara, H. and Nomura. T. (2000). "A study on wheel climb derailment (1st report, results of basic experiments using model truck)," Transactions of the Japan Society of Mechanical Engineers, Series C, Vol. 66, No. 652 , pp. 68-75.
4. Braghin, F., Bruni, S. and Diana, G. (2006). "Experimental and numerical investigation on the derailment of a railway wheelset with solid axle," Vehicle System Dynamics, Vol. 44, No. 4, pp. 305-325.
5. Ishida, H., Matsuo, M. and Fujioka, T. (2005). "Safety Assessment Method of Railway Vehicle under Oscillatory Wheel Load Fluctuation," Transactions of the Japan Society of Mechanical Engineers, Series C, Vol. 71, No. 702, pp. 100-107.
6. RTRI (1993). Manual for the speed-up test of train on conventional railways (in Japanese), pp. 67-78, RTRI.
7. Research Committee of MLIT and RTRI, Research Report on Prevention of Flange-Climb Derailment at Low Speed on Sharp Curve (in Japanese), (2004), p. 23, Research Committee of MLIT and RTRI.
8. Timoshenko, S.P. and Goodier, J.N. (1970). "Theory of Elasticity Third Edition," McGraw-Hill, pp. 414-420.
9. Kalker, J.J. (1979). "Survey of Wheel-Rail Rolling Contact Theory," Vehicle System Dynamics, Vol. 8, No. 4, pp. 317-358.
10. The Japan Society of Mechanical Engineers (1994). Dynamics of railway vehicle (in Japanese), pp. 20-29, Denkisha Kenkyukai.
11. p. 118 in Reference (1).